Jinst

Published by IOP Publishing for Sissa Medialab

Received: *November 30, 2025*
Accepted: *January 23, 2026*
Published: *March 5, 2026*

17TH Topical Seminar on Innovative Particle and Radiation Detectors
Siena, Italy
15–19 September 2025

Mechanical challenges of the innermost layers of ePIC Silicon Vertex Tracker

M.T. Camerlingo [a] on behalf of the ePIC collaboration

[a] *INFN Sezione di Bari,*
Via Orabona 4, 70125 Bari, Italy

E-mail: mariateresa.camerlingo@ba.infn.it

Abstract: At the BNL Electron Ion Collider, the electron Proton/Ion Collider (ePIC) experiment intends to primarily investigate a broad and variegated QCD and Nucleon physics plan, requiring novel and high-performing detectors. An example is its Silicon Vertex Tracker (SVT). Its innermost barrel layers consist of bent radiation-hardened 65 nm CMOS imaging Monolithic Active Pixel sensor chips, minimizing the material budget and multiple scattering effects in the region close to the beam interaction point. The chips are being realised using TPSCo 65 nm CMOS imaging technology and the stitching technique in flat 300 mm wafers. The mechanical bending occurs outside the company and during the assembly of the detector layers. Their design presents several mechanical and cooling challenges faced in synergy with the ALICE ITS3 project. Moreover, the SVT layers will cover cylindrical lateral surfaces with larger radii than ITS3 layers, which drives the need for dedicated R&D and solutions for large radii. For example, in SVT, the radius of the first layer is ∼38 mm, whereas the ITS3 design foresees a ∼19 mm radius. The bending procedure and the local mechanical structure have been validated and optimised on 50 µm-thick silicon dummies. The successive steps consist of assembling a multi-layer mock-up to finalise its construction procedure, and a mechanical and thermal mock-up to perform the thermal and wind tunnel tests. The last prototype will be equipped with temperature sensors and heaters, which mimic the temperature distribution when the power is supplied. The measurements will validate the design of the final detector, and they will be compared with the ongoing simulations.

Keywords: Particle tracking detectors (Solid-state detectors); Detector design and construction technologies and materials; Overall mechanics design (support structures and materials, vibration analysis etc)

© 2026 The Author(s). Published by IOP Publishing Ltd on behalf of Sissa Medialab. Original content from this work may be used under the terms of the Creative Commons Attribution 4.0 licence. Any further distribution of this work must maintain attribution to the author(s) and the title of the work, journal citation and DOI.

https://doi.org/10.1088/1748-0221/21/03/C03007

2026 JINST 21 C03007

Contents

1 Introduction 1

2 ePIC silicon tracker system 1

3 SVT-IB design and its mechanical challenges 4

4 Characterisation studies and design validation 7

5 Conclusions 9

1 Introduction

The electron Proton/Ion Collider (ePIC) experiment will start to operate in late 2034 or early 2035 at the BNL Electron Ion Collider (EIC) [1], where electron and ion beams will collide at high instantaneous luminosity (10^{33}–10^{34}cm^{-2} s^{-1}). The wide ion species (protons-Uranium) and centre-of-mass energy (20–140 GeV) ranges, as well as highly polarized electron and light-hadron beams, will allow to study quantum chromodynamics (QCD) and nucleon properties, such as: the nucleon tomography; the interaction of quarks and gluons in the nuclear medium; the quark confinement; the properties of high-density gluon states; and the origin of the nucleon mass and spin.

The ePIC apparatus will be equipped with proven and novel technologies. It will be organized in a central detector (figure 1-top), which will be an approximately 10-meter long cylinder, with additional instrumentation, including beam monitors and zero degree calorimeter, that extends to up to 45 m in each direction down the EIC beamline. The main features of the central detector are [2]: a 1.7 T superconducting magnet for curving the trajectories of charged particles produced in the EIC collisions; high-precision silicon detectors for tracking particle trajectories in the magnetic field; calorimeters for measuring the energy of electromagnetic particles with high resolution; a suite of particle identification technologies for determining the quark content of particles over a wide range of energies; additional calorimeters at the outer radius of the central detector dedicated to the measurement of "jets"-collimated sprays of particles that arise when a high energy electron scatters off a quark in a proton or ion. A streaming data readout will be used, exploiting AI/ML techniques for data compression. In addition to the data acquisition system, several AI/ML models have already been considered for integration into other levels of the experiment, such as calibration and analysis.

2 ePIC silicon tracker system

In the tracker system of the central detector, the tracking surfaces are equipped with silicon Monolithic Active Pixel Sensors (MAPS) and Micro Patterned Gaseous Detectors (MPGD) as shown in figure 1-bottom. The silicon detectors cover the inner parts, closer to the interaction point. They make up the Silicon Vertex Tracker (SVT). It is subdivided into: Inner Barrel (IB), including the three innermost cylindrical lateral surfaces (or layers: L0, L1, and L2 in table 1); Outer Barrel (OB), representing the fourth and fifth layers (L3, and L4); and, finally, the SVT disks. In general, the SVT design shows several innovative aspects, both in the sensor technology and mechanics.

2026 JINST 21 C03007

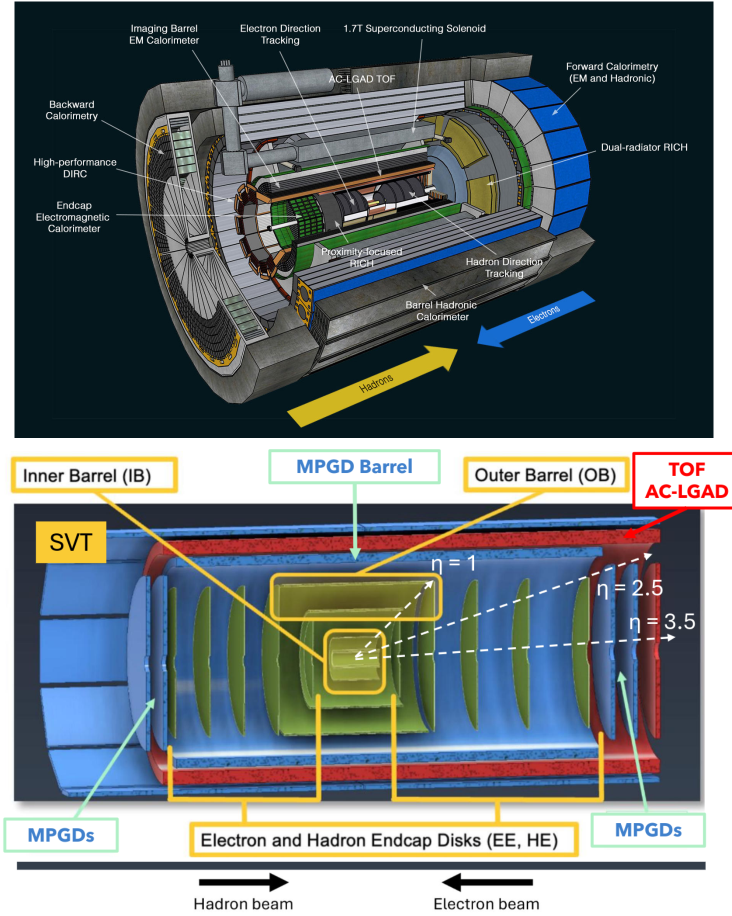

Figure 1. Sketch of the ePIC central detector where the sub-systems are specified (top) and scheme of tracking surfaces of the ePIC tracker system (bottom).

Table 1. Geometry of SVT-IB. The radii are still not the final ones, they might coherently change with the pipe radius.

Layer	Radius (mm)	Single sensor area (mm^2)	Number of sensors per half-layer
L0	~38	266×58.7	2
L1	~50	266×78.3	2
L2	~126	266×97.8	4

Sensor technology. The 65 nm CMOS imaging MAPS sensor [3] is quite a novel technology in the field of vertex tracking. ALICE ITS3 [4] will be the first detector to be equipped with it, followed by ePIC SVT. Indeed, in 2021, the technology was qualified to be used in HEP experiments as a tracker. Compared to the 180 nm process, the 65 nm technology allows a higher in-pixel logic density, reduced material thickness, and lower input capacitance of the collector electrodes, granting a higher signal-to-noise ratio and lower power consumption. In 2023, large-scale demonstrators were realised by TPSCo [5] within 300 mm wafers to assess the stitching technique [6]. The stitching technique

2026 JINST 21 C03007

overcomes the geometrical limitations of the lithographic masks. It is used to create the power and I/O connections among smaller sensor units, called Repeated Sensor Units (RSU). Figure 2 shows the block diagram of the most recent prototypes, called MOSAIX (awaiting their delivery). They will be the first full-working sensors with the final sizes for covering the ITS3 and SVT-IB layers. An RSU includes a matrix of squared ~ 20 µm-pitch pixels, in-pixel and peripheral-matrix logic. The stitched backbones share the power and data I/Os among RSUs. Specifically, the power is symmetrically distributed from the two short sides (or end-caps), minimising the possible voltage drops along the entire segment and optimising the voltage management. Whereas, all the data transmission components are concentrated in the left end-cap (LEC), oriented to the ePIC hadron end-cap.

From the previous engineering run, the ALICE collaboration performed irradiation studies [8] on some MOSS [9] sensors, with $\sim 1.4 \times 26\,\text{cm}^2$ size, showing the technology can efficiently operate up to 10^{13} MeV neutron equivalent flux and Total Ionising Dose higher than those expected at EIC. These results make the 65 nm CMOS imaging technology perfectly suitable for the SVT. The final SVT IB will be equipped with the ALICE ITS3 final sensors, whereas OB and disks will be covered by EIC-LAS sensors derived from the ALICE design.

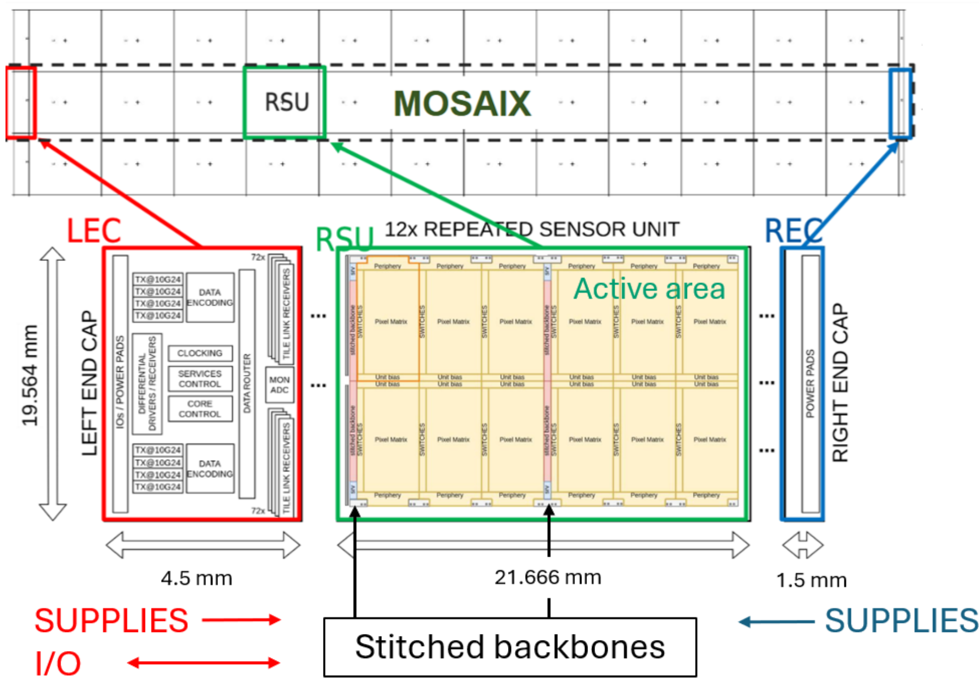

Figure 2. Block diagram of the MOSAIX prototypes, same as the final SVT-IB (and ITS3) sensors. Reproduced from [7]. The Author(s). CC BY 4.0.

Mechanics. The SVT mechanics and cooling system have to assure a perfect alignment, low material budget, and safe sensor operation temperature. The overall common SVT aspects are: ultra-light structures made by carbon foam and fibers, wire bonding for connections, and an air cooling system. The relative material budget (X/X_0) of the total tracker should be less than 5%. The ITS3 and SVT sensors will operate at room temperature.

2026 JINST 21 C03007

3 SVT-IB design and its mechanical challenges

In figure 3-left, the SVT-IB detector design is inspired by the ALICE ITS3 project [4]. It implements non-conventional solutions to minimise the material budget, multiple scattering effects, and dead areas in the region close to the beam interaction point. However, at the same time, they represent challenges in terms of mechanics and services. These are: asymmetrical design; wafer-scale sensors bent into a cylindrical shape (figure 3-left) at target radii; ultra-light structures that can keep the bent sensors in place; and air cooling.

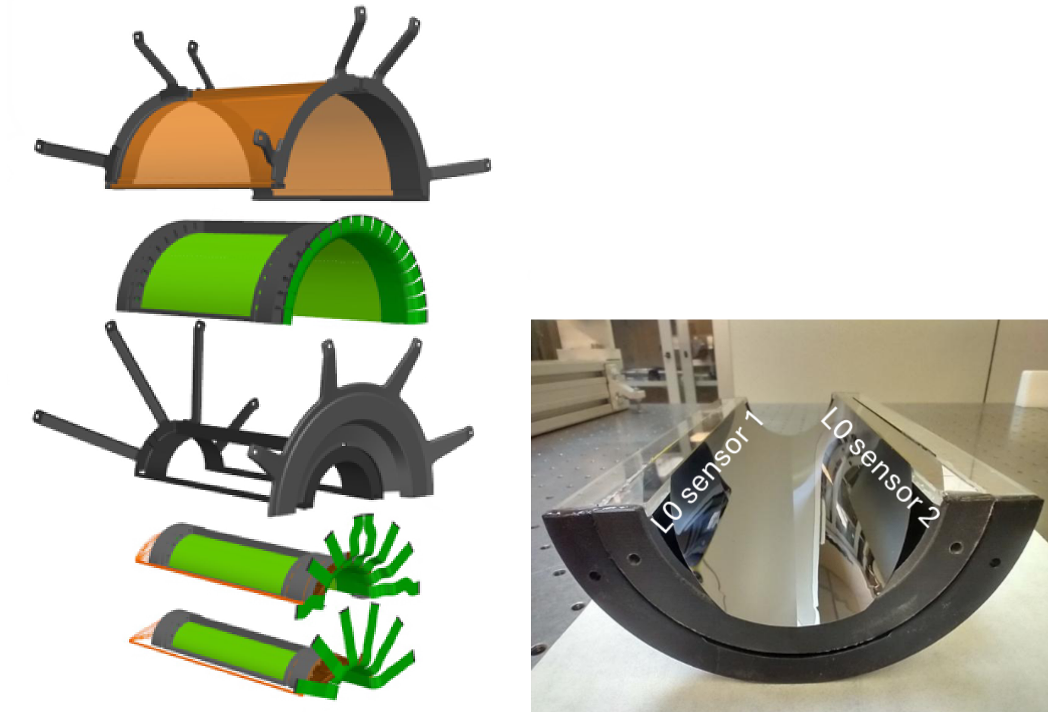

Figure 3. SVT IB design (left) where the MAPSs and flexible printed circuits (FPC) are represented in green, the ultra-light mechanical structure in grey, and a protective/cooling-confinement skin in orange. A picture of the {L0; L1} half-barrel mock-up (right), made by silicon blank dummies and local mechanical structure using alternative materials.

2026 JINST 21 C03007

Asymmetrical design. The SVT-IB is split into two halves, also called half-barrels. Figure 3-left shows the most recent SVT-IB half-barrel design. Along the beam direction, its design is asymmetrical to reduce the material budget at the electron end-cap side, i.e. along the way of the scattered electrons. It directly affects the design of the data transmission and cooling systems.

Wafer-scale sensors and bending procedure. The design in figure 3-left, where wafer-scale sensors and peripheral supports directly define the tracking surfaces, drastically reduces the dead regions and materials budget. The first innermost half-barrel mock-up is shown in figure 3-right, made by four silicon blank dummies, two for each half-cylindrical lateral surface (or layer). In the SVT-IB L0 and L1 layers, the two corresponding sensors are aligned and connected when they are still flat, before bending (figure 4-left). This assembly procedure enables a design in which sensor pairs share the

same local support ("central" longeron) with a width of a few millimeters, avoiding more complex local supports and the alignment of curved objects.

During the alignment, parallelism is prioritized, as a large tilt can affect the chances of successful wire bonding, since the sensor and flexible printed circuit (FPC) pads may be at different azimuthal angles. Our reasonable target is 50 µm pitch, but ongoing performance simulations will determine the final pitch value.

For the sensor connection, a commercial kapton tape is under investigation. Short-term results show that no air bubbles are permanently trapped between the tape and sensors (or silicon blank dummies), and no significant cuspids are present after the bending for the thickness combination of 70 µm kapton tape and 50 µm-thick dummies.

After the tape placement, a long side of the sensor pair is temporarily fixed on a mandrel. This mandrel can (slowly) rotate, and, using a mylar foil as a guide, the sensor pair rolls up around it [4]. Figure 4-right shows the first moments of the bending rolling up of a pair of silicon blank dummies.

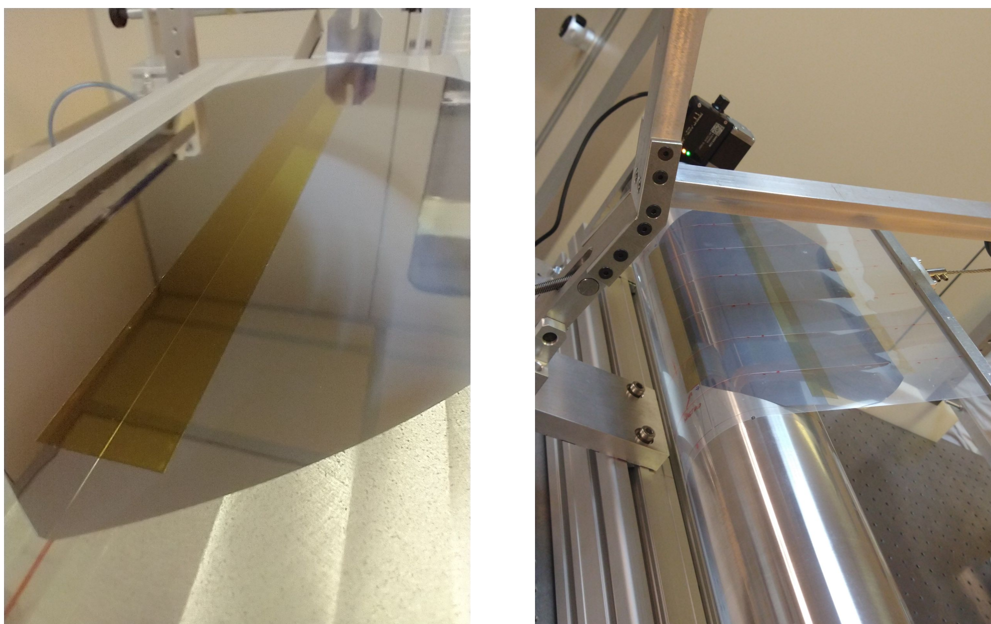

Figure 4. Picture of the tape placement (left) and bending (right).

Wire bonding to flexible printed circuit. After the sensor pair is completely anchored to the mandrel, the mandrel motion stops. After few minutes, the rotation reverses to unroll the mylar foil from the mandrel. Then, polyimide FPCs are aligned with respect to the sensor pair and secured on the mandrel close to the end-caps in order to wire-bond the electric connections between the sensors and them. The FPCs allow power and data transmissions, across the stitched backbones, among RSUs and outside. The entire mandrel with the secured sensor pair and FPCs is moved under the wire-bonding machine. The mandrel is progressively rotated before performing a wire-bonded interconnection at a different azimuthal angle with respect to the previous one. Figure 5 shows the outcomes of the procedure just described where the mandrel and alignment screw are visible.

2026 JINST 21 C03007

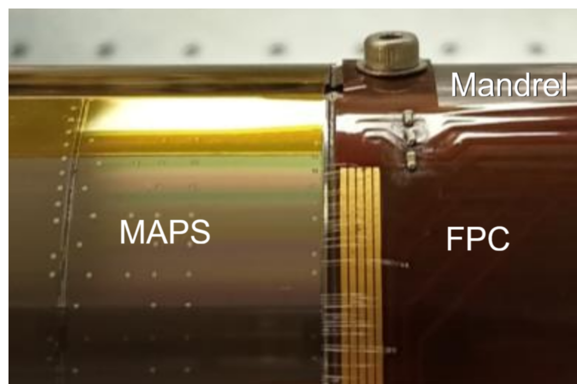

Figure 5. Example of wire-bonded interconnections on curved surfaces performed using the setup available at INFN Bari laboratory.

Ultra-light structure and gluing. For each of the two innermost half-layers, ultra-light supports, comprising three longerons, and two half-rings of different carbon foams (figure 6), are glued using Araldite 2011 on the boundaries of the sensors connected in a pair, i.e. the "central" longeron is glued on the top of the connection kapton tape. All the two half-rings and three longerons are glued in a single step. During the gluing and curing, the ultra-light supports are aligned and held in position by external skeleton structures (similar to those in figure 7) that are removed at the end of glue curing. The next version of these external skeleton structures will be compatible with the presence of the already wire-bonded FPCs.

The ultra-light local supports can not constrain the bent sensors alone. Therefore, an intermediate rigid support between L1 and L2 is present, as visible in figure 3-left. It is glued on the L1 half-layer when it is still constrained on the mandrel. After that, the {support; L1 half-layer} object is removed and glued on top of the L0 half-layer while anchored on its mandrel. The described assembly procedure will soon be executed in the upcoming multi-layer mock-up that will include carbon foam local supports.

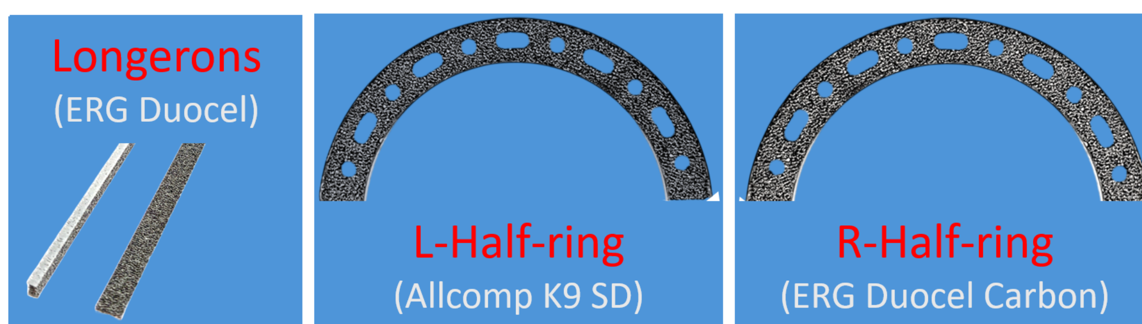

Figure 6. Components of the local structure of a L0 or L1 half-layer. These are made from two types of open-cell reticulated vitreous carbon foams, Allcomp K9 standard density (SD) and ERG Duocel, partially covered by carbon fleeces to facilitate the glue distribution and increase the contact surfaces.

Air cooling. The main advantages of air cooling are lowering the material budget and removing potential damage due to coolant spills. As with the entire SVT mechanics, the cooling system design is also asymmetrical and it takes into account that the air inlet should be on the LEC side to flow

2026 JINST 21 C03007

Figure 7. Central longeron placement during the local structure gluing, with the current version of the skeleton structures for holding the longerons and half rings.

2026 JINST 21 C03007

the coolest air to the expected hottest spots. The cooling design also has to protect the wire bond connections. Then, a series of air ducts channels the air just to the sensors. In the SVT-IB detector, the air convection is not the only method to guarantee an operative temperature between 25°C and 30°C and a maximum gradient ≤ 10°C. The half-rings, made from carbon foam, also dissipate heat by thermal conduction. A high-thermally conductive foam (Allcomp K9 SD) dissipates the heat from the LECs, where the highest power density is expected. A less expensive and lower conductive foam will be used for the half-rings of the right end-caps (RECs) and longerons.[1]

4 Characterisation studies and design validation

Relating to the detector mechanics and cooling system, the vibrations, air flow, and thermal gradients can be sources of random local misalignments. To evaluate these contributions and validate the final detector design, a series of mechanical and thermal studies is planned. The mechanical ones include either finite element simulations (modal, random vibrational, directional deformation, and stress analyses) and the corresponding experimental measurements. The thermal studies also aim to define the operational parameters of the air-cooling system and to investigate the material aging. Similarly, they include simulation studies, air-flow measurements on a dedicated prototype, and thermal expansion tests.

Modal analysis. This analysis serves as a preliminary step for assessing the frequency response and evaluating the effects of random vibrations to determine the structural response to both deterministic and stochastic vibration loads under the detector's operating conditions. Given the geometric aspect ratio and the local half-layer design, comprising three longerons and two half-rings, it is crucial to identify the internal resonant frequencies of the silicon layers and the surrounding support structures. Particular attention is given to the silicon substrates of the detectors, analysed as a function of the radial mode number (radial oscillation index) n. In the first place, the three longerons were assumed to be simple analytic boundaries to determine the approximated trend. After, the displacement map and natural frequency are evaluated using the Finite Element Analysis (FEA) method for several longitudinal and radial (m, n) index combinations (as in figure 8-left), and isotropic or anisotropic silicon cases. These results take into account the structure's elasticity. They are compared with the analytic results in figure 8-right. As visible, for all cases and every value of the longitudinal m index,

[1]The longerons only have a mechanical function.

the frequency increases monotonically at large n, implying that the displacements are localised in the central regions. Moreover, FEA results are systematically shifted towards higher frequencies due to the more realistic boundary conditions than the analytic case. In addition to the numerical FE analysis, measurements on a multi-layer mock-up using a vibration testing machine are being considered.

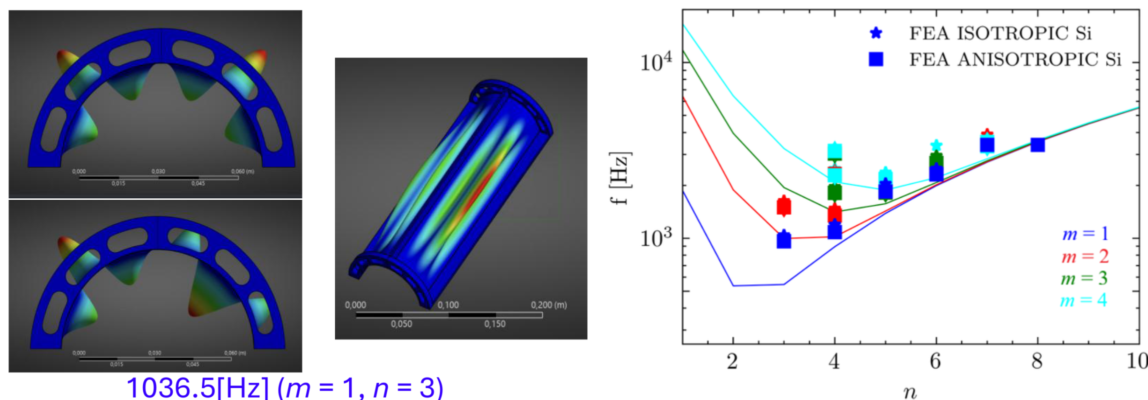

Figure 8. FEA displacement map for (m = 1, n = 3) longitudinal and radial indexes and isotropic silicon case (left). Comparison of the analytic (lines) and FEA (markers) results, natural frequency as a function of the radial index n, where the anisotropic silicon corresponds to the case of a (100) oriented wafer (right).

Thermal simulation. Preliminary static temperature and heat exchange coefficient distributions between the surfaces of a {L1; L0} quarter-barrel have been simulated, assuming that the sensor's power consumption is equal to 40 mW/cm^2 plus 0.8 W/cm^2 (equal to half of the most recent prediction of the maximum LEC's power consumption), an air inlet coming from LEC to REC, and 15 m/s air speed. In figure 9-left, the air enters from the three oval-shaped holes at 300 K (~ 27°C). Along the path to the opposite end-cap, the air temperature increases, slightly exceeding the 10°C temperature gradient requirement. However, the highest temperature is 52°C at the LEC (figure 9-left), confirming that the air convective method is not enough to lower the temperature at the LEC. The heat exchange coefficient map (figure 9-right) shows the zones where the heat exchange is less efficient. To recover the map disuniformities, design modifications specific to the inlet holes and mainfold are being evaluated for the final version of the cooling system.

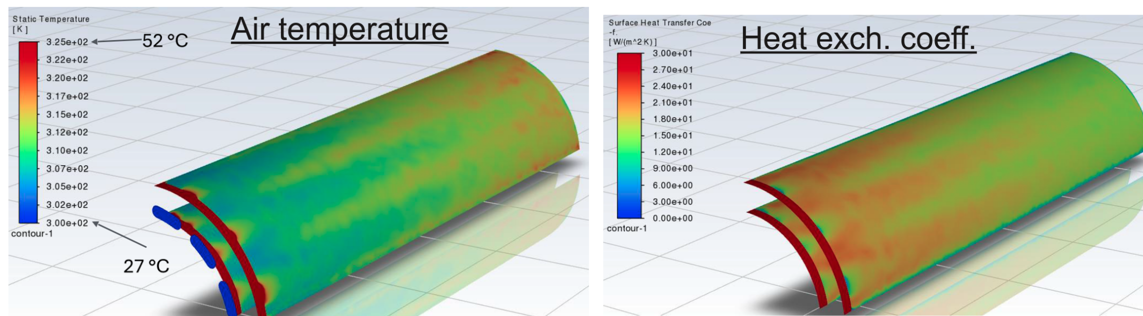

Figure 9. Air temperature (left) and heat exchange coefficient (right) simulated with the assumptions described in the main text.

2026 JINST 21 C03007

Directional deformation and stress. The total displacement variance is evaluated as the quadrature sum of the RMS contributions from airflow-induced vibration, random (seismic and cultural) noise, and thermo-elastic deformation due to short-term temperature fluctuations. The contributions will be evaluated in the next thermal expansion and vibrational tests. Based on the preliminary simulations, the tolerated total displacement is of the order of few µm.

Thermal expansion test. This test evaluates the thermal expansion compatibility of the assembled components made of different materials, and the effects of accelerated aging of the mechanical structure in harsher conditions. Scans with slow and rapid temperature variations are in the program for the next multi-layer mock-up still made of silicon blank dummies and without bonded FPCs but with carbon foam and fleece local structures, in a Genviro 030LC chamber [10].

Air-based cooling performance and vibrational tests. The experimental tests include air-based cooling performance and vibrational tests using a wind tunnel on a dedicated prototype built with silicon blank dummies (with heaters integrating), bonded FPCs, proper carbon foam supports, and air ducts to determine the working air velocity to safely operate the sensors and validate the air-cooling system design. The prototype will be equipped with temperature probes (PT1000 sensors) [11] to measure the temperature and its gradient in several points of the half-lateral surfaces.

5 Conclusions

The developments of ePIC SVT detector are carried out in synergy with ALICE ITS3 combining with a programme of dedicated R&D on ultra-light, integrated mechanics, cooling and electrical services, crucial to the realization of a truly next-generation vertex tracker. The SVT Inner Barrel will be a vertex tracker assembled with bent MAPS, similar to ALICE ITS3. Its design and assembly have required customised solutions. More detailed simulations are in production to guide the next thermal and mechanical tests on dedicated mock-ups. In conclusion, we are now at the final steps of this preparatory phase leading up to MOSAIX sensor characterization and detector design finalisation. The final detector is expected to be installed and finally commissioned in the second-half of 2032 at BNL EIC.

Acknowledgments

The authors gratefully acknowledge the pioneering work, technological advancements, and shared results of the ALICE ITS3 team, which were fundamental for setting up the ePIC SVT R&D studies.

References

[1] R. Abdul Khalek et al., *Science Requirements and Detector Concepts for the Electron-Ion Collider: EIC Yellow Report*, *Nucl. Phys. A* **1026** (2022) 122447 [arXiv:2103.05419].

[2] ePIC collaboration, https://www.bnl.gov/eic/epic.php.

[3] G. Aglieri Rinella et al., *Optimization of a 65 nm CMOS imaging process for monolithic CMOS sensors for high energy physics*, *PoS* **Pixel2022** (2023) 083.

[4] ALICE collaboration, *Technical Design Report for the ALICE Inner Tracking System 3 — ITS3; A bent wafer-scale monolithic pixel detector*, CERN-LHCC-2024-003 (2024).

2026 JINST 21 C03007

[5] Tower Partners Semiconductor Co., https://towersemi.com/tpsco/.

[6] D. Cohen, E. Koltin, M. Ilovich Ayelet and A. Shacham, *Stitching design rules for forming interconnect layers*, United States Patent US 6,225,013 B1 (2021).

[7] P. Vicente Leitao *Development of the MOSAIX chip for the ALICE ITS3 upgrade*, 2025 *JINST* **20** C06001.

[8] A. Kluge, *ALICE - ITS3 — A bent, wafer-scale CMOS detector*, *Nucl. Instrum. Meth. A* **1082** (2026) 170722.

[9] P. Vicente Leitao et al., *Development of a Stitched Monolithic Pixel Sensor prototype (MOSS chip) towards the ITS3 upgrade of the ALICE Inner Tracking system*, 2023 *JINST* **18** C01044.

[10] Genviro 030LC chamber, https://galli2europe.com/en/prodotto/genviro-large-climate-cell/.

[11] PT1000 sensors, https://www.ist-ag.com/en/products/minisens-pt1000-class-f01-optimized-esd-design.